International Journal of Biological Macromolecules 298 (2025) 139860

Contents lists available at ScienceDirect

International Journal of Biological Macromolecules

journal homepage: www.elsevier.com/locate/ijbiomac

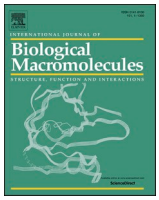

Biomimetic bone cartilage scaffolds based on trilayer methacrylated hydroxyapatite/GelMA composites for full-thickness osteochondral regeneration

Yu Zhong [1], Xia Cao [1], Ming Huang, Yun Lei [*], Ai-Lin Liu [*]

Department of Pharmaceutical Analysis, Higher Educational Key Laboratory for Nano Biomedical Technology of Fujian Province, The School of Pharmacy, Fujian Medical University, Fuzhou 350122, China

ARTICLE INFO

Keywords:
Osteochondral defect
Biomimetic scaffold
Nanohydroxyapatite
GelMA
Full-thickness regeneration

ABSTRACT

Since cartilage injury is often accompanied by subchondral bone damage, conventional single-phase materials cannot accurately simulate the osteochondral structure or repair osteochondral injury. In this work, a gradient gelatin-methacryloyl (GelMA) hydrogel scaffold was constructed by a layer-by-layer stacking method to realize full-thickness regeneration of cartilage, calcified cartilage and subchondral bone. Of note, to surmount the inadequate mechanical property of GelMA hydrogel, nanohydroxyapatite (nHA) was incorporated and further functionalized with hydroxyethyl methacrylate (nHA-hydroxyethyl methacrylate, nHAMA) to enhance the interfacial adhesion with the hydrogel, resulting in better mechanical strength akin to human bone. Specifically, the **b**iomimetic **nHA**MA/Gel**MA** (B-nHAMA) scaffold involved a pure GelMA top layer for cartilage, a 30/70% (*w*/w) nHAMA/GelMA intermediate layer for calcified cartilage, and a 70/30% (w/w) nHAMA/GelMA bottom layer for subchondral bone. This B-nHAMA scaffold exhibited optimal porosity (continuous-gradient pore size), mechanical performance (Young's modulus, 181.48 ± 29.94 kPa), biodegradability (degradation rate in 25 day, 66.04 ± 7.19%) and swelling properties (swelling ratio in 25 h, 424.8 ± 9.9%) that cater to osteochondral tissue environment. It also showed excellent biocompatibility, cell adaptability, chondrogenic and osteogenic properties, leading to effective osteochondral regeneration. Collectively, the developed B-nHAMA scaffold with similar osteochondral microenvironment of trilayered structure could facilitate simultaneous osteochondral regeneration, providing a promising strategy to improve the full-thickness cartilage injury regeneration.

Statement of significance: This research presents a significant advancement in osteochondral repair with the development of a biomimetic B-nHAMA scaffold. The scaffold's design overcomes the inadequate stiffness of gelatin-methacryloyl (GelMA) by incorporating hydroxyethyl methacrylate-functionalized nanohydroxyapatite (nHAMA), enhancing interfacial adhesion and achieving mechanical strength equivalent to human bone. Through a layer-by-layer stacking approach, the B-nHAMA scaffold features a gradient composition that replicates the anisotropic nature of osteochondral tissue, with distinct layers tailored for cartilage, calcified cartilage and subchondral bone. Its biomimetic structure, closely resembling native cartilage in physicochemical and osteogenic properties, positions the B-nHAMA scaffold as a potent therapeutic candidate for the full-thickness repair of osteochondral defects, offering a clinically viable solution.

1. Introduction

Osteochondral defect refers to the absence or damage of cartilage and underlying bone tissue, often caused by osteoarthritis or traumatic injury, posing an obstinate challenge with a lack of effective treatment, due to avascularity, anisotropic physiological characteristics and inadequate regeneration capacity [1,2]. Traditional surgical treatments, such as microfracture, osteochondral autografts and allografts, and autologous cell transplantation, have been proposed in clinical practice [3,4]. However, persistent issues including graft failure, high cost, and formation of fibrocartilage and subchondral bone remain a concern [5,6]. Currently, biomimetic tissue engineering has been regarded as a

* Corresponding authors.
E-mail addresses: leiyun@fjmu.edu.cn (Y. Lei), ailinliu@fjmu.edu.cn (A.-L. Liu).
[1] Yu Zhong and Xia Cao contributed equally to this work.

https://doi.org/10.1016/j.ijbiomac.2025.139860
Received 30 September 2024; Received in revised form 12 January 2025; Accepted 12 January 2025
Available online 13 January 2025

versatile tool for osteochondral regeneration [7]. Hydrogels have been employed as a substitute for both soft and hard supporting tissue, such as gelatin, alginate, collagen, poly(ethylene glycol)diacrylate, *etc.* [8–10]. Thereinto, gelatin-methacryloyl (GelMA), a gelatin derivative, stands out for its photocrosslinking capability, excellent biocompatibility and tunable biodegradability in engineered osteochondral composites [11,12]. Nevertheless, the native stiffness of GelMA is often insufficient to meet the requirements of osteochondral regeneration [13]. To enhance the mechanical properties of GelMA, nanohydroxyapatite (nHA), an inorganic component abundant in calcified cartilage or subchondral bone, has been incorporated due to its biocompatibility, biodegradability, osteoconductivity and osteoinductivity [14], which make it an ideal agent for hydrogel enhancement. Zhang *et al.,* [15] reported that nHA could reduce the pore size of hydrogel and facilitate the reconstruction of the network, resulting in the improvement of tensile and compressive strengths. Moreover, Yang et al., [16] displayed that grafting hydroxyethyl methacrylate (HEMA) to the surface of nHA (nHA-hydroxyethyl methacrylate, abbreviated nHAMA) could endow it with photoreactivity and improve the colloidal stability of nHAMA/hydrogel prepreparation solution. Roy et al., [17] demonstrated that HEMA functionalization enhanced the interfacial adhesion between nHA and chitosan hydrogel, achieving better mechanical strength comparable to that of human bone. Hence, with the introduction of photocrosslinkable nHAMA, the inorganic-organic hybrid hydrogels possess enhanced mechanical performance and are expected to accelerate osteochondral regeneration.

Due to its anisotropic physiological characteristics, osteochondral tissue presents multiple gradients in cell type, matrix composition, architecture and mechanical properties from the superficial cartilage to the intermediate calcified cartilage and into the deep subchondral bone, necessitating scaffolds that can replicate this intricate gradient [18,19]. To this end, various heterogeneous constructs with tailored biomechanical and biochemical gradients have been developed to imitate the osteochondral microenvironment, with the aim of repairing full-thickness cartilage injuries. For example, Dai *et al.,* [19] displayed a stem cell-loaded dual-layer GelMA hydrogel for three-dimensional (3D) bioprinting of heterogeneous construct for osteochondral regeneration. The bottom layer, with a higher mechanical modulus, was loaded with melatonin to induce bone regeneration, while the upper layer, with a lower rigidity, was equipped with kartogenin to promote chondrogenesis. This approach promoted cell adaptation and adhesion, augmented mechanical strength, and facilitated simultaneous regeneration of cartilage and bone. Zhang *et al.,* [15] reported a three-layer alginate hydrogel scaffold fabricated by 3D printing, consisting of a pure hydrogel cartilage layer, an interlayer for calcified cartilage with 40/60% (*w*/w) nHA/hydrogel and a subchondral bone layer with 70/30% (w/w) nHA/hydrogel. This gradient nHA/hydrogel scaffold possessed sufficient mechanical property and controlled degradability, which facilitated simultaneous regeneration of cartilage and subchondral bone. Although allowing for customized production, the high cost of 3D bioprinting technology, the demanding and meticulous preparation of bioinks, and the intricate manufacturing processes involved in creating gradient structured scaffolds pose significant challenges to its broader practical implementation. On the contrary, using layer-by-layer stacking method in mild gelling condition can realize rapid, efficient and economical manufacturing, but it is difficult to control of its elaborate structure.

To achieve full-thickness osteochondral defects regeneration and streamline the preparation process, a **b**iomimetic **nHA**MA/Gel**MA** (B-nHAMA) scaffold was developed using a layer-by-layer stacking method. As shown in Scheme 1, this three-layer scaffold featured a pure GelMA top layer for cartilage, an intermediate layer with 30/70% (w/w) nHAMA/GelMA for calcified cartilage, and a 70/30% (w/w) nHAMA/GelMA bottom layer for subchondral bone. Compared with the monolayer homogeneous nHA/GelMA composite [20] and three-layer cell-laden nHA/GelMA composite [21], the B-nHAMA scaffold possessed continuous-gradient pore size, high mechanical performance, desired biodegradability and swelling behaviors, making it suitable for tissue engineering applications. Both *in vitro* and *in vivo* studies demonstrated its superiority in biocompatibility, chondrogenic and osteogenic properties, and osteochondral regeneration effect. The B-nHAMA scaffold could achieve simultaneous regeneration of cartilage, calcified cartilage and subchondral bone, which is expected to be a viable treatment option for osteochondral defects.

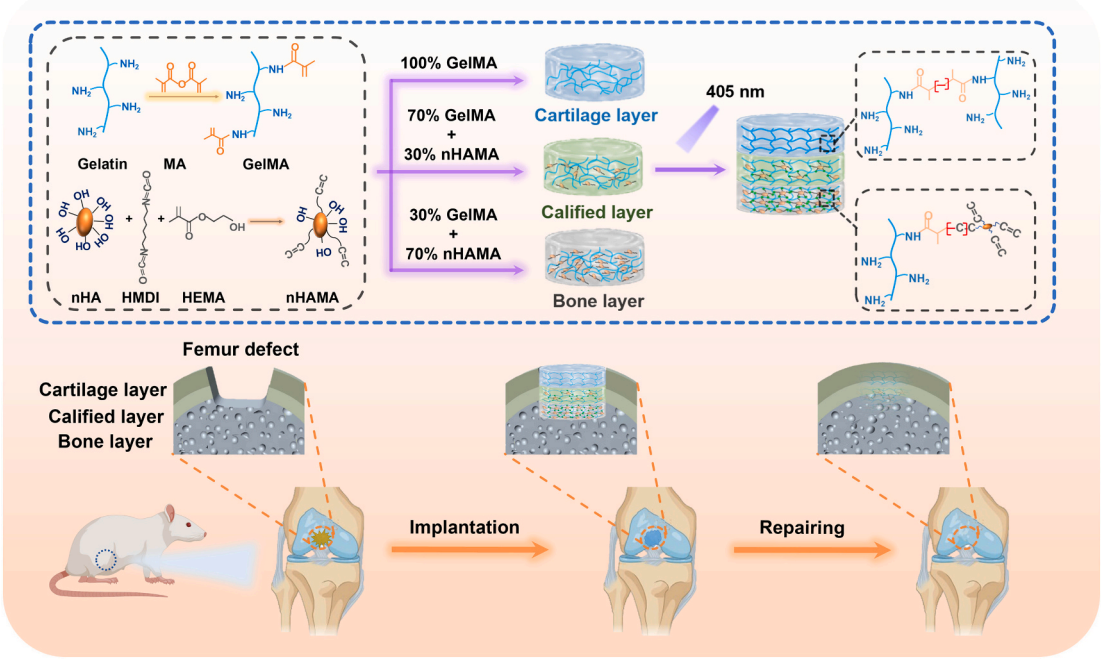

Scheme 1. Schematic illustration of biomimetic bone cartilage scaffolds based on trilayer methacrylated hydroxyapatite/GelMA composites for full-thickness osteochondral regeneration.

2. Experimental sections

Reagents, apparatus, preparation of GelMA, GelMA hydrogel, nHAMA and various scaffolds, swelling performance test, degradation performance test, *in vitro* and *in vivo* biological studies were provided in Supplementary Information.

3. Results and discussion

3.1. Characterization of scaffolds

3.1.1. ^1H NMR spectra of GelMA and gelatin

The chemical reaction between gelatin and methacrylic anhydride (MA) was analyzed by ^1H nuclear magnetic resonance (^1H NMR) spectroscopy, and the results were shown in Fig. S1. Two peaks of GelMA appeared at 5.32 ppm and 5.55 ppm, which were attributed to vinyl in MA, indicating successful grafting of methyl acrylamide group on gelatin. In addition, the signal at 2.89 ppm belonged to the methylene proton of -NH_2, and the degree of substitution (*DS*%) of the methyl acrylamide group on gelatin could be calculated by the formula $DS\% = (1 - I_{\text{GelMA 2.89}}/I_{\text{Gelatin 2.89}}) \times 100\%$, where *I* represented the peak area. The *DS*% of the methyl acrylamide group on gelatin was 70%, which was basically consistent with the literature [22].

3.1.2. Characterization of nHA and nHAMA

nHAMA was synthesized by grafting HEMA to hydroxyl groups of nHA *via* hexamethylene diisocyanate (HMDI). For morphology, both nHA (Fig. S2A) and nHAMA (Fig. S2B) manifested an ellipsoidal morphology. The average size of nHA and nHAMA was 96.48 nm and 100.98 nm, respectively. To confirm the chemical groups, Fourier transform infrared (FT-IR) spectra of nHA, HEMA and nHAMA were characterized. In Fig. S2C, the characteristic peaks of nHAMA (3400 cm^{-1} and 1037 cm^{-1} corresponding to '-OH' and '-PO_4^{3-}' groups, respectively) were basically unchanged in nHA. After graft of HEMA, the peaks at 2945 cm^{-1} for '-CH_2' groups, 1643 cm^{-1} for 'C=C' groups and 1570 cm^{-1} for 'N-H' groups could be observed in nHAMA. Further, to assess the crystalline structure, X-ray diffraction (XRD) spectra of nHA and nHAMA were obtained. In Fig. S2D, with regard to the characteristic diffraction of (002), (102), (210), (211), (112), (300), (222), (213) and (004), there was almost no difference between nHA and nHAMA, and the diffraction peaks well matched with the standard card (JCPDS No. 09-0432), indicating the introduction of HEMA did not change the crystallinity, crystalline phase or the intrinsic properties of nHA. Then, thermogravimetric analysis (TGA) was carried out to quantify the amount of organic phase (HMDI-HEMA) coupled to nHAMA *via* comparing the differences of the total weight loss between nHA and nHAMA. As shown in Fig. S2E, *ca.* 37.31 wt% of HMDI-HEMA was grafted to nHAMA. The above results indicated that nHAMA was successfully prepared.

The comparative photoreactivity of nHA and nHAMA was shown in Fig. S2F–H. nHA and nHAMA were uniformly dispersed in the photopolymerization solution without ultraviolet (UV) irradiation (Fig. S2F). After UV irradiation and static settlement for 5 min, nHA was still evenly dispersed, whereas nHAMA produced visible precipitates (Fig. S2G). Subsequently, after UV irradiation and 15 min of placement, nHA was still homogeneously dispersed in the polymerization solution, while nHAMA produced more precipitation (Fig. S2H). The results showed that nHAMA was photoreactive after grafting HMDI-HEMA on the surface of nHA.

3.1.3. Morphological characterization

The content of nHAMA incorporated in hydrogels is a key to accurately replicating the osteochondral architecture and determining the effectiveness of treatment. To comprehensively investigate the impact of nHAMA on physiochemical and biological properties of gradient scaffolds, five groups of scaffolds were prepared, including GelMA (pure GelMA), 30% nHA (30% (*w*/w) nHA/70% (w/w) GelMA), 30% nHAMA (30% (w/w) nHAMA/70% (w/w) GelMA), 70% nHAMA (70% (w/w) nHAMA/30% (w/w) GelMA) and B-nHAMA. The morphologies of these synthesized scaffolds (Fig. 1A–E) were characterized by scanning electron microscope (SEM). All scaffolds exhibited a porous and interconnected structure, which facilitated the exchange of nutrients, oxygen and waste products. With the incremental incorporation of nHA or nHAMA content, the pore sizes decreased gradually. The pore sizes of GelMA, 30% nHA, 30% nHAMA and 70% nHAMA scaffolds were 87.9 ± 5.6 μm, 43.8 ± 1.6 μm, 52.9 ± 6.4 μm and 20.7 ± 2.5 μm, respectively. As reported in the literature [23], micropores (<50 μm in diameter) help promote the adsorption and retention of proteins on the scaffold surface and are critical for subsequent cell adhesion, while macropores (>50 μm in diameter) provide channels for the diffusion of nutrients and cells. To recapitulate the osteochondral holistic tissue, the pore size of the B-nHAMA decreased gradually from top to bottom (Fig. 1Ei–iii), which is conducive for maintaining a balance between nutrient diffusion and cell adhesion and proliferation.

3.1.4. Mechanical property characterization

Excellent mechanical property is an important clinical criterion for bone scaffolds, and the mechanical strength that well matches native bone tissues is desirable. As such, compressive tests were performed on various scaffolds, and the compressive stress-strain curves were depicted in Fig. 1F. Compared with pure GelMA, the mechanical strength of 30% nHA and 30% nHAMA was obviously improved, with the 30% nHAMA showing superiority (Fig. 1G). The increment in Young's modulus might be attributed covalent bonding between the HEMA chains on nHAMA and GelMA, resulting in the improved interfacial bonding [24]. However, the 70% nHAMA group exhibited relatively low mechanical strength. This can be explained by two factors: firstly, the precursor solution of 70% nHAMA was opaque, leading to the reduced transmittance and the incomplete UV irradiation within the scaffold, thereby weakening its load-bearing capacity. Secondly, the low amount of GelMA was insufficient to support and distribute the load effectively. Of note, the B-nHAMA scaffold displayed the highest Young's modulus with 181.48 ± 29.94 kPa, indicating the gradient scaffolds enabled effective stress distribution and possessed robust mechanical performance. The hardness of cartilage ranges from 100 kPa to 6200 kPa [25–27], and only the B-nHAMA scaffold fall within this range. Although the Young's modulus of the pure GelMA layer in B-nHAMA scaffold was much lower than that of native cartilage, the soft GelMA is expected to enable cells to sense changes in stiffness and facilitate cartilage regeneration [28]. The 30% nHAMA layer in B-nHAMA scaffold mainly plays a vital role of mechanical support, while the 70% nHAMA layer is expected to promote bone growth. This outcome may be attributed to the remarkable structural similarity between the B-nHAMA scaffold and osteochondral tissue, highlighting the inorganic-organic hybrid hydrogels' mechanical tunability and the B-nHAMA scaffold's potential for clinical bone regeneration.

3.1.5. Water absorption capacity and degradation studies

High water absorption capacity in hydrogels is beneficial for cell migration, interactions and mass transport [15]. As shown in Fig. 2A, all scaffolds rapidly swelled upon immersion in phosphate buffer saline (PBS, 1×, pH 7.4) and reached swelling equilibrium within 7 h. The swelling ratio (*SR*) of the scaffolds decreased with increasing nHA or nHAMA content (Fig. 2B), due to restricted water molecule diffusion resulting from the incorporation of nHA or nHAMA. In addition, larger pores allowed easier water molecule entry, thus increasing water content of the scaffolds, which was consistent with the SEM observations (Fig. 1A–E). Compared with the 30% nHA group, the 30% nHAMA group displayed higher *SR*, indicating that grafting hexamethylene diisocyanate (HMDI)-HEMA on the nHA surface could enhance the water absorption of the scaffold. As previously reported, the *SR* of osteochondral tissues ranged between 50% and 1600% [15,29–31], and thus the B-

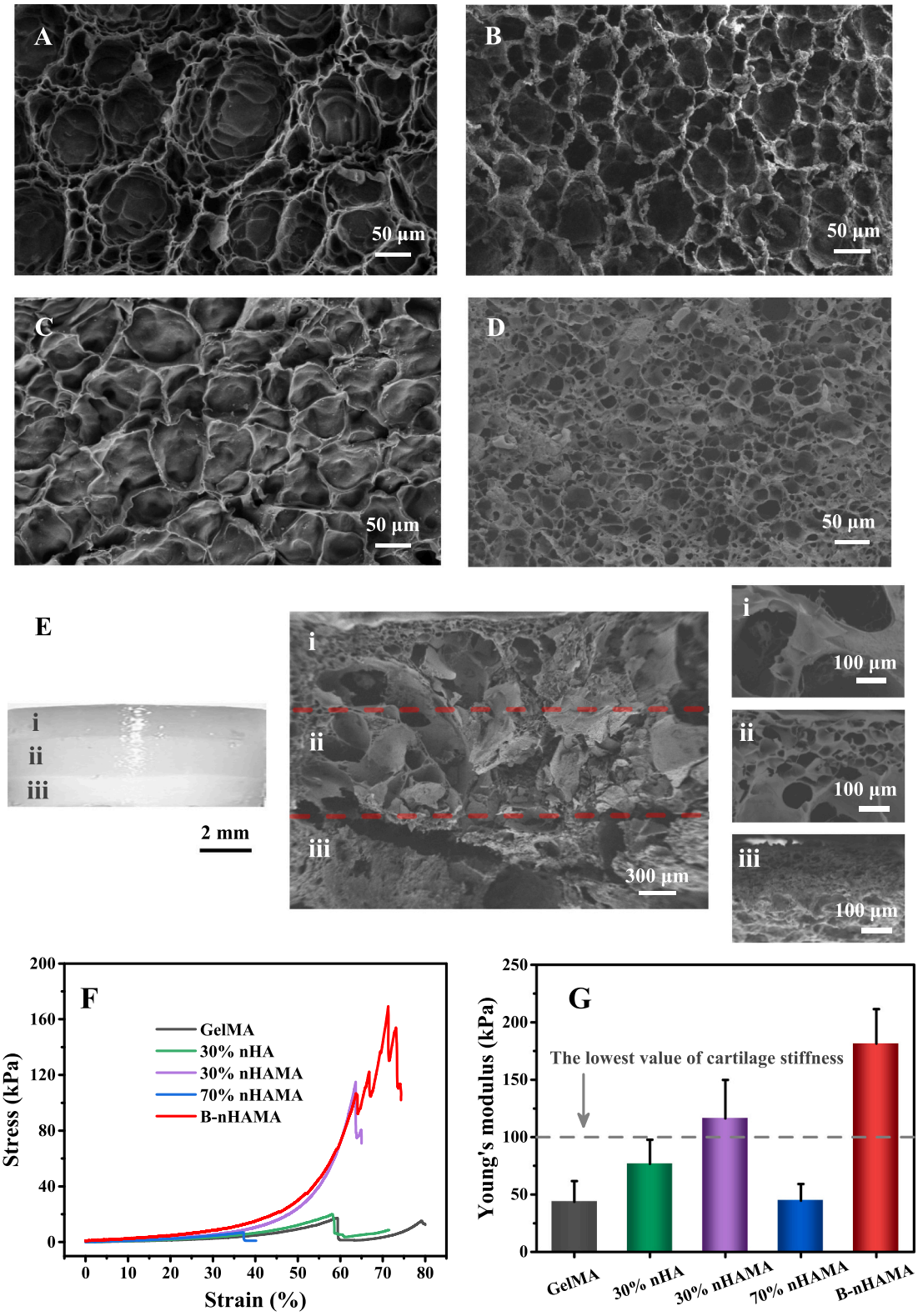

Fig. 1. SEM images of GelMA (A), 30% nHA (B), 30% nHAMA (C) and 70% nHAMA (D). (E) Photograph (left), SEM image (middle) and high-resolution SEM images (right) of B-nHAMA. Ei: GelMA; Eii: 30% nHAMA; Eiii: 70% nHAMA. Stress-strain curves (F) and Young's modulus (G) of GelMA, 30% nHA, 30% nHAMA, 70% nHAMA and B-nHAMA.

nHAMA scaffold's *SR* of 424.8 ± 9.9% met these requirements.

Moreover, it is preferential for an implantable scaffold to achieve a balance between the material biodegradation rate and the tissue growth rate. *In vitro* degradation test showed that all scaffolds displayed different degradation behaviors. As shown in Fig. 2C, GelMA scaffolds exhibited the fastest degradation rate (*DR*). With the introduction of nHA or nHAMA, the *DR* obviously decreased by the 25th day (Fig. 2D). With the increase of the amount of nHAMA, the *DR* reduced, owing to

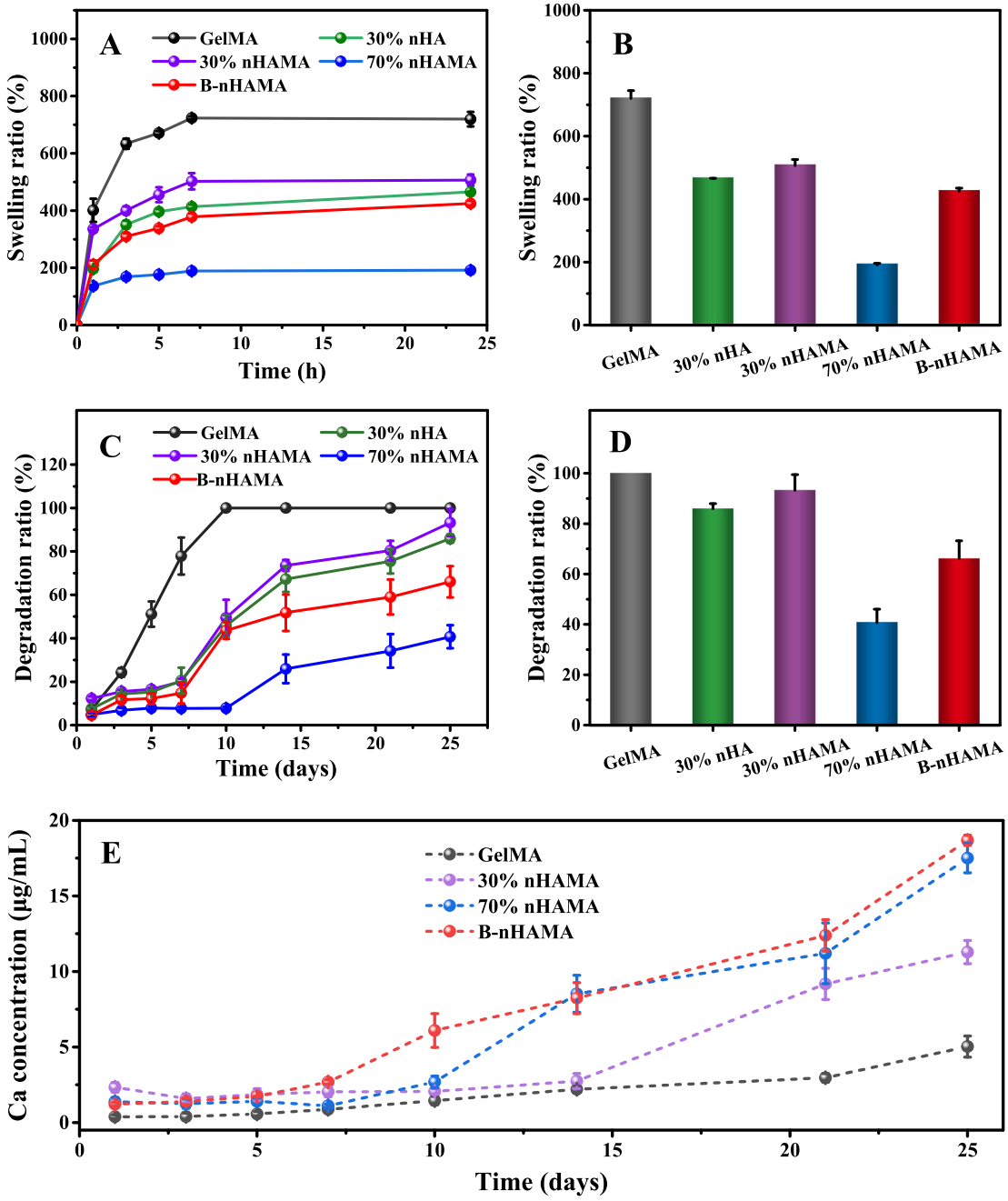

Fig. 2. Characterizations of swelling and degradation of various scaffolds. (A-B) Swelling behaviors of various scaffolds soaked in PBS for 24 h. (C-D) Degradation ratio of various scaffolds in type II collagenase over 25 days. (E) Release profile of calcium ions from various scaffolds.

the smaller pore size confirmed by SEM (Fig. 1A–E). The GelMA layer at the top of the B-nHAMA scaffold degraded faster than the middle 30% nHAMA and bottom 70% nHAMA layers, matching with faster cartilage regeneration compared to subchondral bone [32]. Cartilage formation needs the structure support provided by the underlying bone. As such, the results were in accord with the strategic design of the B-nHAMA scaffold with a relatively slow biodegradation rate. Meanwhile, the release profile of calcium ions during the degradation process was measured. As shown in Fig. 2E, the B-nHAMA scaffold could sustainably release calcium ion for over 25 days without any burst release. The GelMA scaffold slowly released a small amount of calcium ion derived from gelatin. In 30% nHAMA and 70% nHAMA groups, the calcium ion concentration slightly decreased after 3 days, which probably due to the readsorption of calcium ion by the external frameworks. After that, the 30% nHAMA and 70% nHAMA scaffolds could continuously release calcium ion for over 25 days, but with a little white material dissolved out. In addition, we tested the stiffness of B-nHAMA scaffolds before degradation experiment, and the stiffness was 40.60 ± 0.28 g. Subsequently, we soaked the B-nHAMA scaffolds in PBS containing 0.02 U/mL type II collagenase. After 25 days, the hardness of the B-nHAMA scaffolds was reduced to 30.51 ± 0.69 g, due to its *DR* (66.04 ± 7.19%). These attributes are instrumental in promoting osteochondral regeneration.

3.2. *In vitro biological study of B-nHAMA*

3.2.1. *Biocompatibility study*

The biocompatibility of the scaffolds is a vital prerequisite for tissue

engineering applications. The biocompatibility study was conducted to assess the cell proliferation, viability and adhesion on various scaffolds using the cell counting kit-8 (CCK-8) assay, calcein acetoxymethyl ester/propidium iodide (calcein AM/PI) staining, and fluorescein isothiocyanate (FITC)-phalloidin staining and morphological observation, respectively. The CCK-8 assay results (Fig. 3A) showed the increased optical density (*OD*) values at 450 nm for mouse embryo osteoblast precursor cells in subclone 14 (MC3T3-E1) co-cultured with various scaffolds from day 1 to day 5, indicating that the cells were proliferated normally. The *OD* values of the 30% nHAMA group were little or slightly higher than the 30% nHA group, indicating that the grafting HMDI-HEMA on the nHA surface did not impair the biocompatibility of nHA. The 70% nHAMA group also displayed high *OD* values on day 5, showing that the incorporation of nHAMA did not obviously affect cell proliferation. Notably, the gradient structure in B-nHAMA scaffold closely resembled that of osteochondral tissue, leading to high cell proliferation, suggesting excellent biocompatibility with MC3T3-E1 cells. Calcein AM/PI staining (Fig. 3B) revealed negligible red fluorescence, indicating no obvious cytotoxicity of the scaffolds over 5 days. Of note, the B-nHAMA group's fluorescence intensity and cell density closely resembled with the control group, highlighting its superiority in cell proliferation and tissue regeneration.

According to the aforementioned results, the biosafety of 30% nHAMA scaffold and 30% nHA scaffold was basically identical (Fig. 3A and B), indicating that the grafting of HMDI-HEMA on the surface of nHA did not change the cell viability on nHA. And the physicochemical properties of 30% nHAMA scaffold were superior than that of 30% nHA scaffold (Figs. 1G, 2B and D). Hence, only GelMA, 30% nHAMA, 70% nHAMA and B-nHAMA scaffolds were assessed in downstream experiments, that is, cell adhesion experiment, osteogenic differentiation experiment and *in vivo* experiment. For cell adhesion evaluation, SEM images of MC3T3-E1 cells after 24 h (Fig. 3C) revealed comparable cell densities among the GelMA, 70% nHAMA and 30% nHAMA groups. Notably, the B-nHAMA scaffold exhibited the highest cell attachment with an elongated and polygonal cell morphology, manifesting its capacity to boost cell adhesion. Similarly, for FITC-phalloidin staining (Fig. S3), the cytoskeleton of cells attached to the GelMA scaffold was not fully unfolded, whereas the cytoskeleton of the 30% nHAMA scaffold was wide and the cells were well spread. The cells cultured on the 70% nHAMA scaffold showed minor antennae protruding. In contrast, in the B-nHAMA group, cells demonstrated a uniform distribution across the scaffold, indicative of superior cell adaptation. Collectively, the B-nHAMA scaffold offers commendable biocompatibility and cell adaptability toward MC3T3-E1 cells.

3.2.2. Osteogenic differentiation

The osteogenesis potential of the scaffolds was assessed. Firstly, alkaline phosphatase (ALP) activity, an early biomarker indicative of the osteogenic phenotype and crucial for the onset of bone matrix mineralization, was evaluated. The B-nHAMA scaffold exhibited a notably larger and denser ALP-stained area (Fig. 4A), and quantification analysis confirmed its enhanced ALP activities (Fig. 4B), underscoring its superior osteogenic potential. Subsequently, alizarin red S (ARS) staining, an indicator of the late-stage osteogenic efficiency reflecting extracellular matrix mineralization, was carried out. The ARS staining results in Fig. 4C–D displayed significantly increased matrix mineralization in the B-nHAMA group, further manifesting its robust osteogenesis potential. Lastly, to further elucidate the underlying molecular mechanisms, quantitative real-time polymerase chain reaction (qRT-PCR) analysis was employed to evaluate the expression levels of key cartilage-related genes, including collagen type II (COL-II) (Fig. 4E) and SRY-box transcription factor 9 (SOX-9) (Fig. 4F), as well as bone-associated genes, including collagen type I (COL—I) (Fig. 4G) and runt-related transcription factor 2 (RUNX-2) (Fig. 4H), after differentiation for 14 and 21 days. The upregulation of these marker in the B-nHAMA group was consistent with the ALP and ARS staining results, confirming the scaffold's potential to support osteogenic functions at all stages. According to reports [33–36], we hypothesized that B-nHAMA scaffold promote

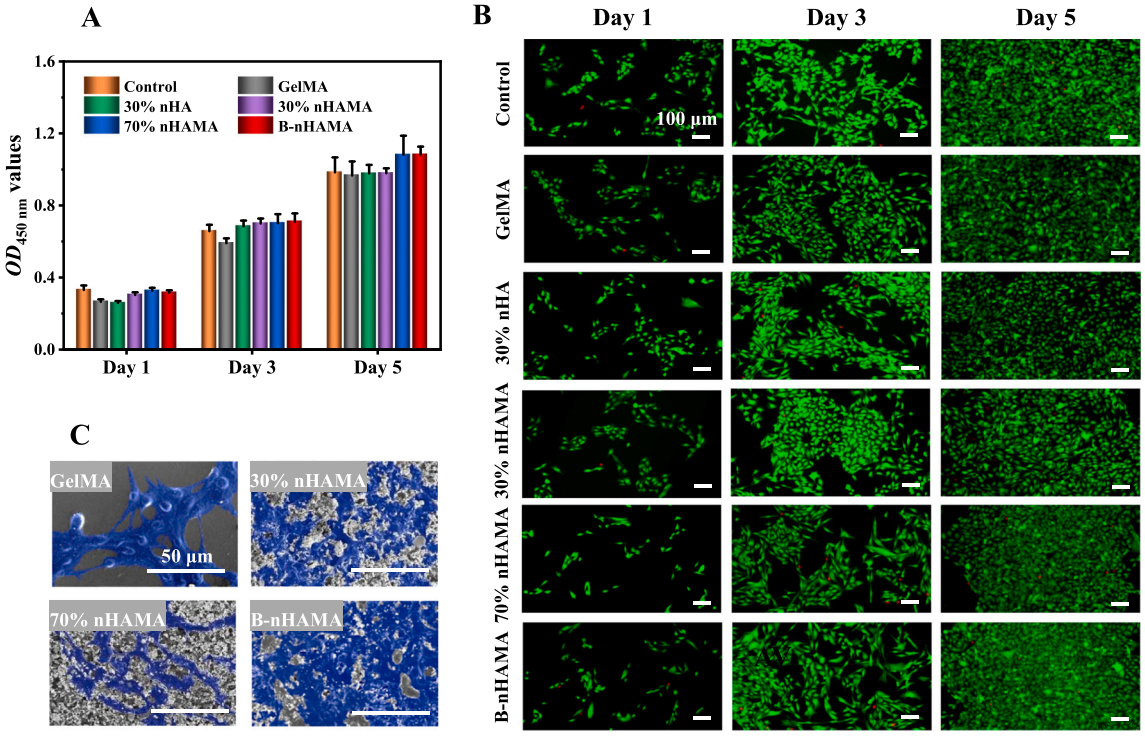

Fig. 3. Cell proliferation activity, viability and adhesion on various scaffolds. (A) Cell proliferation activity of MC3T3-E1 cells assessed by CCK-8 assay after incubation for 1, 3 and 5 days. (B) Cell viability evaluated by calcein AM/PI staining after MC3T3-E1 cells co-cultured with different scaffolds for 1, 3 and 5 days. (scale bars = 100 μm). (C) SEM images of MC3T3-E1 cells co-cultured with different scaffolds for 24 h to reflect the cell adhesion (scale bars = 50 μm).

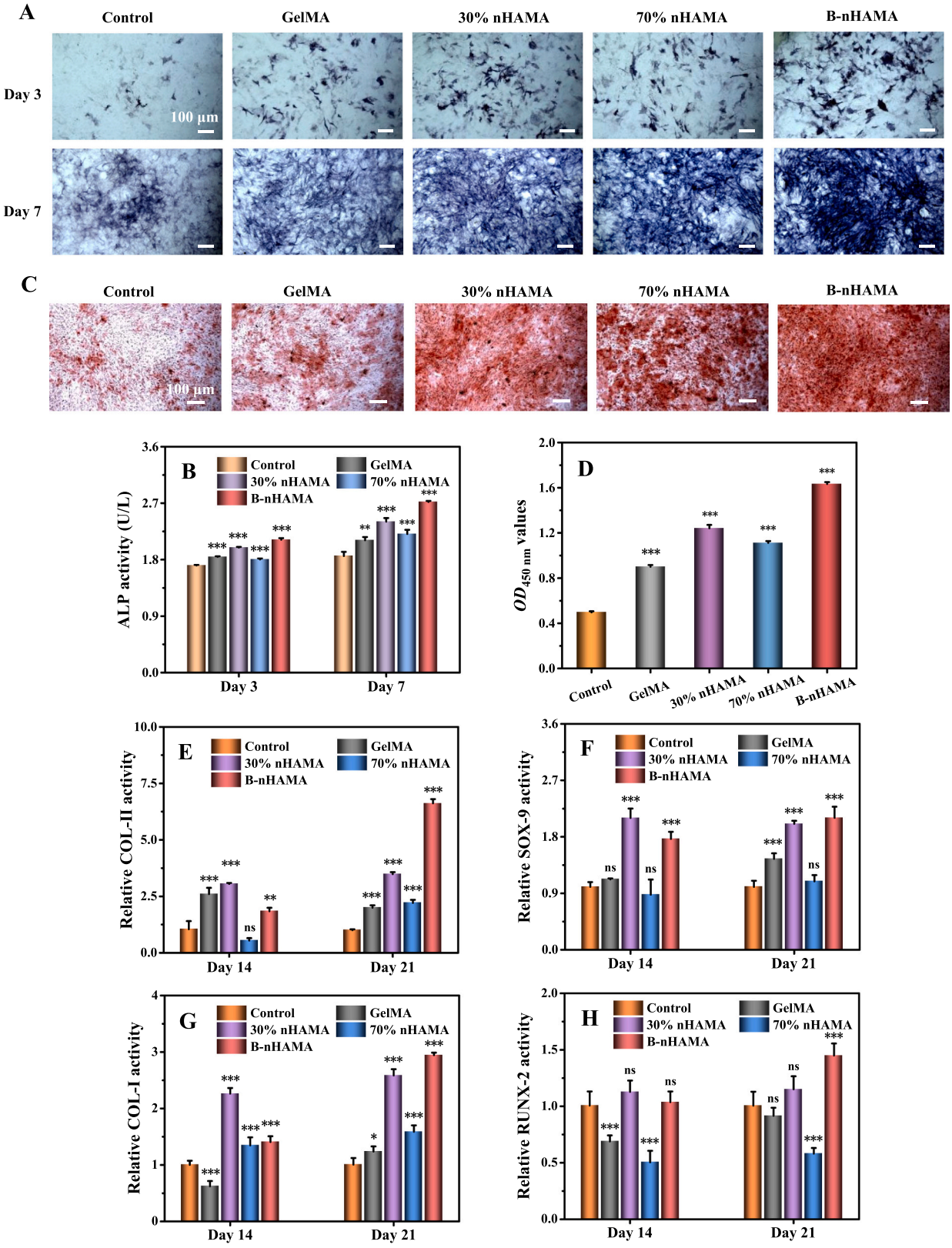

Fig. 4. *In vitro* evaluation of osteogenic differentiation of MC3T3-E1 cells on various scaffolds. ALP staining (A) and quantification (B) of MC3T3-E1 cells cultured for 3 and 7 days (scale bars = 100 μm). ARS staining (C) and quantitative analysis of matrix mineralization (D) of MC3T3-E1 cells cultured for 21 days (scale bars = 100 μm). qRT-PCR analysis of cartilage-related gene expressions including COL-II (E) and SOX-9 (F), and bone-associated gene expressions including COL-I (G) and RUNX-2 (H) after cultivation for 14 and 21 days. The data were presented as mean ± S.D. ($n = 3$). Compared with control group, ***$P < 0.001$, **$P < 0.01$, *$P < 0.05$, ns > 0.05.

chondrogenesis and osteogenesis *via* focal adhesion kinase (FAK), mitogen-activated protein kinase (MAPK) and Wnt/β-catenin signaling pathways. This excellent performance of B-nHAMA scaffold can be attributed to the continuous-gradient pore size, bionic surface stiffness, proper swelling and degradation properties, and the similar osteochondral microenvironment of trilayered structure. Owing to the large pore size of GelMA and gravitational infiltration, MC3T3-E1 cells were prone to locate and attach to the 30% nHAMA layer. Hence, the differentiation capacity of cells on 30% nHAMA scaffold was similar to that of the B-nHAMA scaffold. However, 70% nHAMA scaffold exhibited the worst osteogenic activity, potentially due to its small pore size, low Young's modulus, and unbefitting swelling and degradation rates, and thus limiting the diffusion of nutrients, cell-cell interactions and differentiation capacity. The pure GelMA scaffold was completely degraded in 10 days (Fig. 2C), so the calcium nodules and gene expressions were obviously low in the absence of scaffold, while its ALP expression did not differ much from that of other scaffolds within 7 days. This observation underscores the necessity for a balanced nHAMA concentration within the hybridized hydrogel to effectively stimulate osteogenic differentiation.

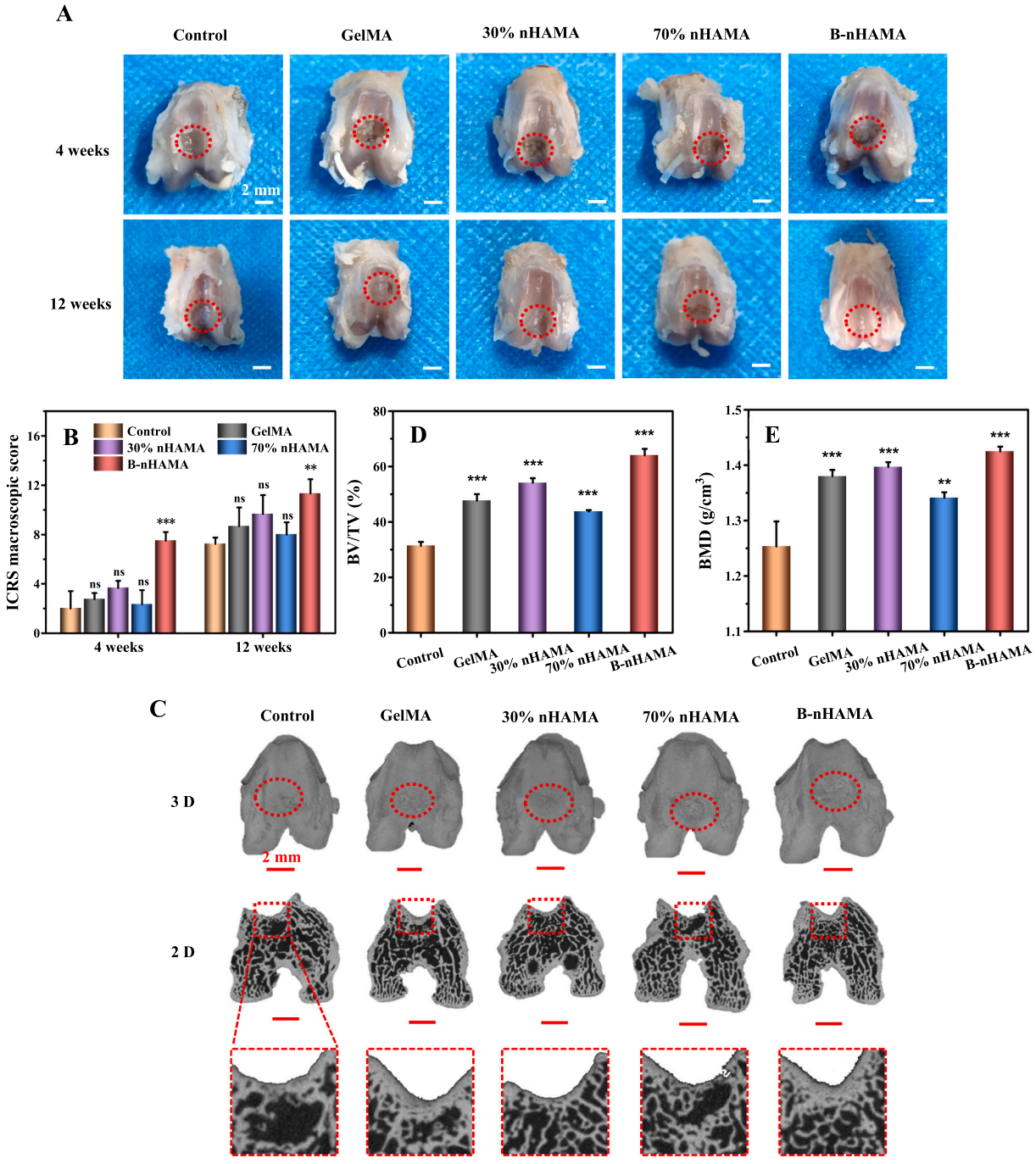

Fig. 5. Simultaneous regeneration of cartilage-subchondral bone in osteochondral defect after implantation. Gross images (A) and ICRS macroscopic score (B) of repair tissues at various scaffolds after 4 and 12 weeks (red circles: surgical area, scale bars = 2 mm). The data were presented as mean ± S.D. (n = 3). Compared with control group, ***$P < 0.001$, **$P < 0.01$, ns > 0.05. Micro-CT images (C) and quantitative analysis of BV/TV (D) and BMD (E) of the newly formed cartilage after 12 weeks. The data were presented as mean ± S.D. (n = 3). Compared with control group, ***$P < 0.001$, **$P < 0.01$. Red ovals: the implantation sites of scaffolds. Red squares: normal and enlarged views of subchondral bone areas where the scaffolds are implanted (scale bars = 2 mm).

3.3. In vivo biological study of B-nHAMA

3.3.1. Gross observations

To ascertain the osteochondral regeneration efficacy of the developed biomimetic scaffold with trilayered structure, which incorporate both biomechanical and biochemical gradients, an *in vivo* biological study was performed to evaluate the scaffolds' capacity to promote tissue regeneration. Osteochondral defect modeling and scaffold implantation were shown in Fig. S4. The rats did not display any infection, and their surgical incised skins healed progressively. Tissue samples were collected at 4- and 12-weeks post-implantation, with the frontal views of the knee joints depicted in Fig. 5A (the circled region indicates the surgical site). In the control group, new tissue appeared in the defect at 4 weeks after surgery, but it differs in color from the surrounding cartilage tissue and presented an obvious depression, indicating incomplete osteochondral regeneration. At week 12, the margin of the defect remained distinguishable from the healthy cartilage with a persistent depression. The regenerated tissue, mainly composed of hyaline cartilage, was transparent but did not match the functionality of native cartilage. In the GelMA group, after 12 weeks, the new tissue had almost filled the entire defect, the color was basically consistent with that of the adjacent cartilage. Half of the defect edges showed complete integration with the host bone, while the other half were either not integrated or exhibited shallow cracks. The 30% nHAMA and the 70% nHAMA groups demonstrated complete defect regeneration after 12 weeks with the color of the new tissue matching the normal cartilage and a smooth surface and blurred border, but minor cracks were observed. In contrast, the B-nHAMA group showed complete defect regeneration after 12 weeks, a smooth tissue surface, no discernible boundary between the regenerated tissues and adjacent cartilage, and without any cracks or other abnormalities. In addition, the regenerated cartilage tissues were scored according to International Cartilage Repair Society (ICRS) macroscopic assessment scale. As illustrated in Fig. 5B, the corresponding ICRS scores of each group increased over time, with the ranking of the groups based on their scores being: B-nHAMA >30% nHAMA > GelMA >70% nHAMA > Control. The results were consistent with the aforementioned *in vitro* osteogenesis results (Fig. 4), demonstrating the increased mechanical properties and tailored swelling and degradation properties could further induce the osteogenesis *in vivo*. And the three-layer B-nHAMA scaffold, which closely replicated the osteochondral microenvironment, showcased a superior osteochondral self-regeneration effect.

3.3.2. Micro computed tomography (micro-CT) analysis

To verify the regeneration effect of the scaffolds, micro-CT imaging was used to evaluate osteochondral regeneration after implantation for 12 weeks. The 3D reconstructed images (the red ovals outline the implantation locations of the scaffolds) and two-dimensional (2D) lateral reconstructed images (the red squares indicate subchondral bone areas where the scaffolds are implanted) were presented in Fig. 5C. In the control group, only few bone trabeculae were formed around the defect site, indicating the limited self-regeneration ability. In the GelMA and 70% nHAMA groups, the trabeculae were irregular and the subchondral bone was not completely regenerated. Conversely, in the 30% nHAMA and the B-nHAMA groups, the trabeculae of the subchondral bone were evenly distributed, and the regenerated new bone tissue of the B-nHAMA group was similar to natural bone tissue in structure and density. Quantitative analysis of micro-CT data further confirmed the superiority of the B-nHAMA scaffold evidenced by its high ratio of bone volume to tissue volume (BV/TV, Fig. 5D) and bone mineral density (BMD, Fig. 5E). These metrics were indicative of the B-nHAMA scaffold's outstanding osteoinductive ability, which was crucial for effectively stimulating the new osteochondral formation.

3.3.3. Histological analysis

Furthermore, the decalcified samples from the repair sites of the osteochondral defects at 4 and 12 weeks post-surgery were assessed by hematoxylin and eosin (HE), safranin O/fast green and Masson staining to evaluate tissue regeneration and integration. For HE staining (Fig. 6A), red or pink mainly represents the cytoplasm and extracellular matrix, and blue or purple usually represents the nucleus. In the control group, fibrous connective tissue was observed in the defect instead of cartilage and subchondral bone, and the defect was not fully filled at 4 weeks. By 12 weeks, although the defect site was completely filled, surface cracks persisted, and partial regeneration of the subchondral bone was noted. In the GelMA, 30% nHAMA and 70% nHAMA groups, the newly formed tissues mainly consisted of fibrous connective tissue at 4 weeks, and the defects were almost completely repaired at 12 weeks. In the B-nHAMA group, at 4 weeks post-treatment, the defect area exhibited no obvious depression, and a thicker repaired cartilaginous layer was observed at 12 weeks. For safranin O/fast green staining (Fig. 6B), the cartilage was stained red, and the subchondral bone was stained blue or green. In the control group, the defect site was not colored at 4 weeks, indicating that the newly formed tissue was neither cartilage nor subchondral bone. By12 weeks, the center of the defect stained red, indicating that the regenerated tissue was mainly cartilage, although the subchondral bone had not been completely restored. In the GelMA group, the cartilage tissue was regenerated well, but persistent surface cracks were observed. In the 30% nHAMA group, by 12 weeks, the cartilage and subchondral bone were basically regenerated, but some cartilage tissue had grown into the subchondral bone, resulting in a less distinct demarcation between local cartilage tissue and subchondral bone. In the 70% nHAMA group, neither cartilage nor subchondral bone had regenerated at 4 weeks. By 12 weeks, regeneration of cartilage and subchondral bone was observed in the central region, whereas the lateral and the lower regions mainly consisted of fibrous tissue, which was not well integrated with the surrounding bone tissue, with obvious boundaries and gaps in some regions. In the B-nHAMA group, both cartilage and subchondral bone were completely regenerated, the subchondral bone was mature and the trabecular bone was arranged regularly, significantly outperforming the other groups. For Masson staining (Fig. 6C), collagen was colored blue, mature bone was colored red, and the newly-formed bone presented a state between blue and red colors. In the control group, the cartilage and subchondral bone were not colored at 4 weeks, however, by 12 weeks, these tissues appeared blue, indicating the regenerated subchondral bone had not yet reached maturity. The 30% nHAMA and 70% nHAMA groups showed partial maturation of the subchondral bones. In contrast, the B-nHAMA group displayed clear demarcation lines between the newborn cartilage and subchondral bone, which were completely fused with the surrounding native bone tissue. According to the Modified O'Driscoll Histology Scoring System (MODHS), the histological scores of the regenerated tissues were ranked as follows: B-nHAMA >30% nHAMA > GelMA >70% nHAMA > Control (Fig. 6D), which was in accordance with ICRS scores, micro-CT findings and *in vitro* osteogenesis results. These histological results further confirmed the optimal osteochondral defect regeneration of the three-layered B-nHAMA scaffold with merits of its excellent mechanical performance, swelling and degradability properties, biocompatibility, cell adaptability, chondrogenic and osteogenic properties. The B-nHAMA scaffold, with its multifaceted advantages, serves as a valid therapeutic option for full-thickness cartilage injury regeneration.

4. Conclusions

In summary, a B-nHAMA scaffold with a gradient stiffness profile from the cartilaginous layer to the subchondral bone layer was developed for the full-thickness regeneration of osteochondral defects. This scaffold had porous microstructures, bionic mechanical capacity, and controlled biodegradability and swelling properties, which are essential for tissue regeneration. The *in vitro* assessments demonstrated its advantages in biocompatibility, cell adaptability, chondrogenic and

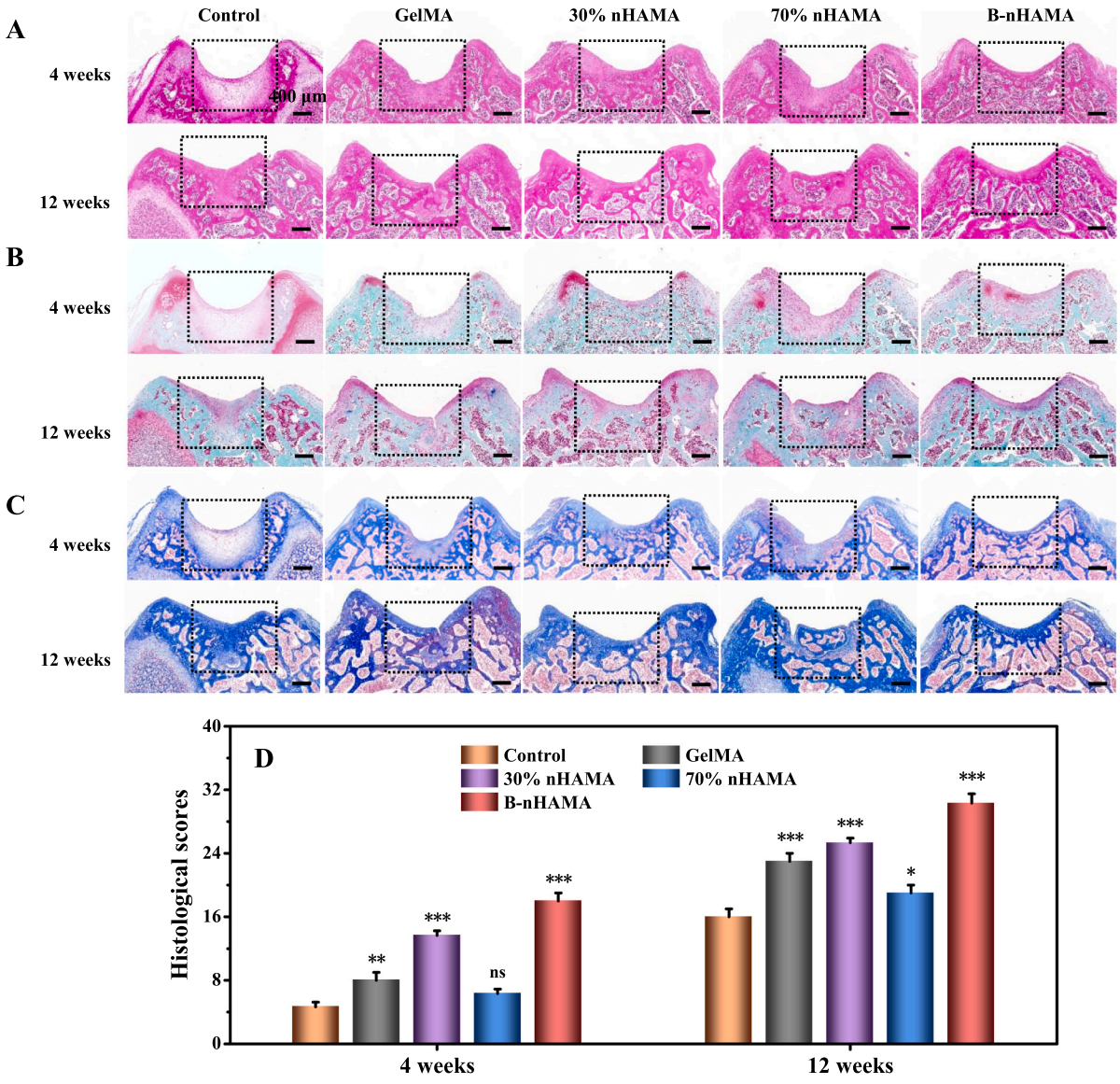

Fig. 6. Histological analysis of the osteochondral defect after implantation at 4 and 12 weeks. HE staining (A), safranin O/fast green staining (B), Masson staining (C) and histological scores (D) of the repair of osteochondral defect (scale bars = 400 μm). Black rectangles: repair area of osteochondral defect. The data were presented as mean ± S.D. (n = 3). Compared with control group, ***$P < 0.001$, **$P < 0.01$, *$P < 0.05$, ns > 0.05.

osteogenic properties. The *in vivo* studies confirmed that the scaffold possessed optimal osteochondral regeneration effects, with simultaneous regeneration of cartilage and subchondral bone within 12 weeks. Additionally, rather than using 3D printing, the photocrosslinkable B-nHAMA scaffold was prepared through a layer-by-layer stacking method. This method to some extent streamlines the complex processes (such as bioink preparation and formulation optimization), achieves shape plasticity and large-scale production, and reduces the manufacture cost, making it more accessible to the basic research or even the preclinical research. Collectively, the cost-effective and easily-acquired B-nHAMA scaffold could match natural cartilage in physiochemical properties and osteogenic properties by meticulously simulating the structure of natural bone cartilage, suggesting the promising clinical potential in full-thickness cartilage injury regeneration.

CRediT authorship contribution statement

Yu Zhong: Writing – original draft, Investigation. **Xia Cao:** Writing – original draft, Investigation. **Ming Huang:** Investigation. **Yun Lei:** Writing – review & editing, Supervision, Project administration. **Ai-Lin Liu:** Writing – review & editing, Supervision, Project administration.

Declaration of competing interest

The authors declare that they have no known competing financial interests or personal relationships that could have appeared to influence the work reported in this paper.

Acknowledgements

The authors gratefully acknowledge the financial support of the National Natural Science Foundation of China (82373838) and Project supported by the Science Foundation of Fujian Province (2020Y4018). The authors would like to thank Yan Hu from the Public Technology Service Center of Fujian Medical University for technical assistance.

Appendix A. Supplementary data

Supplementary data to this article can be found online at https://doi.org/10.1016/j.ijbiomac.2025.139860.

Data availability

The data used in the present study are available from the corresponding author on reasonable request.

References

[1] Z. Gu, J. Wang, Y. Fu, H. Pan, H. He, Q. Gan, C. Liu, Smart biomaterials for articular cartilage repair and regeneration, Adv. Funct. Mater. 33 (10) (2023) 2212561.

[2] K. Kapat, S. Kumbhakarn, R. Sable, P. Gondane, S. Takle, P. Maity, Peptide-based biomaterials for bone and cartilage regeneration, Biomedicines 12 (2) (2024) 313.

[3] D.P. Trofa, I.S. Hong, C.D. Lopez, A.J. Rao, Z. Yu, S.M. Odum, C.T. Moorman 3rd, D.P. Piasecki, J.E. Fleischli, B.M. Saltzman, Isolated osteochondral autograft versus allograft transplantation for the treatment of symptomatic cartilage lesions of the knee: a systematic review and meta-analysis, Am. J. Sports Med. 51 (3) (2023) 812–824.

[4] K. Abe, A. Yamashita, M. Morioka, N. Horike, Y. Takei, S. Koyamatsu, K. Okita, S. Matsuda, N. Tsumaki, Engraftment of allogeneic iPS cell-derived cartilage organoid in a primate model of articular cartilage defect, Nat. Commun. 14 (1) (2023) 804.

[5] C. Zhai, Q. Zuo, K. Shen, J. Zhou, J. Chen, X. Zhang, C. Luo, H. Fei, W. Fan, Utilizing an integrated tri-layered scaffold with titanium-mesh-cage base to repair cartilage defects of knee in goat model, Mater. Design 193 (2020) 108766.

[6] A.R. Martin, J.M. Patel, R.C. Locke, M.R. Eby, K.S. Saleh, M.D. Davidson, M. L. Sennett, H.M. Zlotnick, A.H. Chang, J.L. Carey, J.A. Burdick, R.L. Mauck, Nanofibrous hyaluronic acid scaffolds delivering TGF-β3 and SDF-1α for articular cartilage repair in a large animal model, Acta Biomater. 126 (2021) 170–182.

[7] Y. Cao, H. Zhang, M. Qiu, Y. Zheng, X. Shi, J. Yang, Biomimetic injectable and bilayered hydrogel scaffold based on collagen and chondroitin sulfate for the repair of osteochondral defects, Int. J. Biol. Macromol. 257 (2024) 128593.

[8] P. Jurczak, S. Lach, Hydrogels as scaffolds in bone-related tissue engineering and regeneration, Macromol. Biosci. 23 (11) (2023) 2300152.

[9] X. Qin, Z. Zhao, J. Deng, Y. Zhao, S. Liang, Y. Yi, J. Li, Y. Wei, Tough, conductive hydrogels based on gelatin and oxidized sodium carboxymethyl cellulose as flexible sensors, Carbohydr. Polym. 335 (2024) 121920.

[10] X. Li, S. Sheng, G. Li, Y. Hu, F. Zhou, Z. Geng, J. Su, Research progress in hydrogels for cartilage organoids, Adv. Healthc. Mater. (2024) 2400431.

[11] Y. Zhu, X. Yu, H. Liu, J. Li, M. Gholipourmalekabadi, K. Lin, C. Yuan, P. Wang, Strategies of functionalized GelMA-based bioinks for bone regeneration: Recent advances and future perspectives, Bioact. Mater. 38 (2024) 346–373.

[12] C. Xu, Y. Chang, Y. Xu, P. Wu, C. Mu, A. Nie, Y. Qu, D. Duan, X. Guo, Z. Liu, J. Wang, Z. Luo, Silicon-phosphorus-nanosheets-integrated 3D-printable hydrogel as a bioactive and biodegradable scaffold for vascularized bone regeneration, Adv. Healthc. Mater. 11 (6) (2022) e2101911.

[13] Y. Zhang, M. Sun, T. Liu, M. Hou, H. Yang, Effect of different additives on the mechanical properties of gelatin methacryloyl hydrogel: a Meta-analysis, ACS Omega 6 (13) (2021) 9112–9128.

[14] Y. Zhang, F. Wang, H. Tan, G. Chen, L. Guo, L. Yang, Analysis of the mineral composition of the human calcified cartilage zone, Int. J. Med. Sci. 9 (5) (2012) 353–360.

[15] H. Zhang, H. Huang, G. Hao, Y. Zhang, H. Ding, Z. Fan, L. Sun, 3D printing hydrogel scaffolds with nanohydroxyapatite gradient to effectively repair osteochondral defects in rats, Adv. Funct. Mater. 31 (1) (2021) 2006697.

[16] Y. Yang, T. Xu, Q. Zhang, Y. Piao, H.P. Bei, X. Zhao, Biomimetic, stiff, and adhesive periosteum with osteogenic-angiogenic coupling effect for bone regeneration, Small 17 (14) (2021) e2006598.

[17] P. Roy, R.R.N. Sailaja, Chitosan-nanohydroxyapatite composites: mechanical, thermal and bio-compatibility studies, Int. J. Biol. Macromol. 73 (2015) 170–181.

[18] X. Niu, N. Li, Z. Du, X. Li, Integrated gradient tissue-engineered osteochondral scaffolds: challenges, current efforts and future perspectives, Bioact. Mater. 20 (2022) 574–597.

[19] W. Dai, L. Zhang, Y. Yu, W. Yan, F. Zhao, Y. Fan, C. Cao, Q. Cai, X. Hu, Y. Ao, 3D bioprinting of heterogeneous constructs providing tissue-specific microenvironment based on host-guest modulated dynamic hydrogel bioink for osteochondral regeneration, Adv. Funct. Mater. 32 (23) (2022) 2200710.

[20] S. Zheng, D. Li, Q. Liu, C. Tang, W. Hu, S. Ma, Y. Xu, Y. Ma, Y. Guo, B. Wei, C. Du, L. Wang, Surface-modified nano-hydroxyapatite uniformly dispersed on high-porous GelMA scaffold surfaces for enhanced osteochondral regeneration, Int. J. Nanomed. 18 (2023) 5907–5923.

[21] M. Li, P. Song, W. Wang, Y. Xu, J. Li, L. Wu, X. Gui, Z. Zeng, Z. Zhou, M. Liu, Q. Kong, Y. Fan, X. Zhang, C. Zhou, L. Liu, Preparation and characterization of biomimetic gradient multi-layer cell-laden scaffolds for osteochondral integrated repair, J. Mater. Chem. B 10 (22) (2022) 4172–4188.

[22] X. Zhao, S. Liu, L. Yildirimer, H. Zhao, R. Ding, H. Wang, W. Cui, D. Weitz, Injectable stem cell-laden photocrosslinkable microspheres fabricated using microfluidics for rapid generation of osteogenic tissue constructs, Adv. Funct. Mater. 26 (17) (2016) 2809–2819.

[23] R.A. Perez, G. Mestres, Role of pore size and morphology in musculo-skeletal tissue regeneration, Mater. Sci. Eng. C Mater. Biol. Appl. 61 (2016) 922–939.

[24] Y. Yang, Q. Zhang, T. Xu, H. Zhang, M. Zhang, L. Lu, Y. Hao, J.H. Fuh, X. Zhao, Photocrosslinkable nanocomposite ink for printing strong, biodegradable and bioactive bone graft, Biomaterials 263 (2020) 120378.

[25] C.F. Guimarães, L. Gasperini, A.P. Marques, R.L. Reis, The stiffness of living tissues and its implications for tissue engineering, Nat. Rev. Mater. 5 (5) (2020) 351–370.

[26] L. Fu, L. Li, Q. Bian, B. Xue, J. Jin, J. Li, Y. Cao, Q. Jiang, H. Li, Cartilage-like protein hydrogels engineered via entanglement, Nature 618 (7966) (2023) 740–747.

[27] S. Davis, M. Roldo, G. Blunn, G. Tozzi, T. Roncada, Influence of the mechanical environment on the regeneration of osteochondral defects, Front. Bioeng. Biotechnol. 9 (2021) 603408.

[28] L. Zheng, S. Liu, X. Cheng, Z. Qin, Z. Lu, K. Zhang, J. Zhao, Intensified stiffness and photodynamic provocation in a collagen-based composite hydrogel drive chondrogenesis, Adv. Sci. 6 (16) (2019) 1900099.

[29] F. Zhou, X. Zhang, D. Cai, J. Li, Q. Mu, W. Zhang, S. Zhu, Y. Jiang, W. Shen, S. Zhang, H.W. Ouyang, Silk fibroin-chondroitin sulfate scaffold with immuno-inhibition property for articular cartilage repair, Acta Biomater. 63 (2017) 64–75.

[30] H. Yao, J. Kang, W. Li, J. Liu, R. Xie, Y. Wang, S. Liu, D.A. Wang, L. Ren, Novel β-TCP/PVA bilayered hydrogels with considerable physical and bio-functional properties for osteochondral repair, Biomed. Mater. 13 (1) (2017) 015012.

[31] D. Algul, A. Gokce, A. Onal, E. Servet, A.I. Dogan Ekici, F.G. Yener, *In vitro* release and *in vivo* biocompatibility studies of biomimetic multilayered alginate-chitosan/β-TCP scaffold for osteochondral tissue, J. Biomater. Sci. Polym. Ed. 27 (5) (2016) 431–440.

[32] C. Deng, C. Xu, Q. Zhou, Y. Cheng, Advances of nanotechnology in osteochondral regeneration, WIRES Nanomed. Nanobi. 11 (6) (2019) e1576.

[33] Y. Yang, Q. Zhang, T. Xu, H. Zhang, M. Zhang, L. Lu, Y. Hao, J.H. Fuh, X. Zhao, Photocrosslinkable nanocomposite ink for printing strong, biodegradable and bioactive bone graft, Biomaterials 263 (2020) 120378.

[34] Y. Yang, T. Xu, H.P. Bei, L. Zhang, C.Y. Tang, M. Zhang, C. Xu, L. Bian, K.W. Yeung, J.Y.H. Fuh, X. Zhao, Gaussian curvature-driven direction of cell fate toward osteogenesis with triply periodic minimal surface scaffolds, P. Natl. Acad. Sci. USA 119 (41) (2022) e2206684119.

[35] J. Chen, Y. Qian, H. Li, W. Zuo, W. Sun, D. Xing, X. Zhou, Lysophosphatidic acid/polydopamine-modified nHA composite scaffolds for enhanced osteogenesis via upregulating the Wnt/beta-catenin pathway, ACS Appl. Mater. Interfaces 16 (11) (2024) 13466–13480.

[36] S. Zhu, W. Chen, A. Masson, Y.P. Li, Cell signaling and transcriptional regulation of osteoblast lineage commitment, differentiation, bone formation, and homeostasis, Cell Discov. 10 (1) (2024) 71.